

Article

## Hyperspectral Classification of Savannah Tree Species Using *k*-fold Cross-Validated Non-linear Support Vector Machines

Morteza Shahriari Nia <sup>1,\*</sup>, Daisy Zhe Wang <sup>1</sup>, Milenko Petrovic <sup>2</sup>, Stephanie Ann Bohlman <sup>3</sup> and Paul Gader <sup>1</sup>

<sup>1</sup> Department of Computer and Information Science and Engineering, University of Florida, 432 Newell Dr., Gainesville, Florida 32611, USA

<sup>2</sup> Institute for Human and Machine Cognition, 15 SE Osceola Ave, Ocala, Florida 34471, USA

<sup>3</sup> School of Forest Resources and Conservation, 349 Newins Ziegler Hall, Gainesville, Florida 32611, USA

\* Author to whom correspondence should be addressed; [msnia@cise.ufl.edu](mailto:msnia@cise.ufl.edu)

Received: xx / Accepted: xx / Published: xx

**Abstract:** Identifying savannah species at ecological scale is major milestone in measuring biomass, carbon reserves, drought and invasive species spread predictions. In this paper we perform classification and geo-mapping of tree species from hyperspectral imagery collected using AVIRIS airborne sensors. We provide a comparison of ATCOR and FLAASH and atmospheric corrections. This study classifies four common savannah tree species in Ordway-Swisher Biological Station in north-central Florida, USA. Among predictors we found NDVI, the NIR wavelengths (734.1nm) and removal of water absorption bands to be most useful. Gaussian filter was used to avoid sensor measurements and calibration errors. We studied varieties of the widely popular Support Vector Machines out of which a polynomial kernel outperformed others. Our classification scheme produces accurate predictions of about 98.26% at pixel level. This research was performed as a pilot study for the National Ecological Observatory Network-Airborne Observation Platform protocols.

**Keywords:** Specie classification; Hyperspectral; Savannah; Support Vector Machines; Ordway-Swisher Biological Station; High spatial and spectral resolution; Pixel-level classification; National Ecological Observatory Network; Airborne Observation Platform protocols; NEON-AOP

## 1. Introduction

Mapping tree species by remote sensing techniques is an essential step in understanding how species play roles at ecological scale. This will enable us to study land covers, climate change, invasive species, plant competitions, predict fire potentials and spreading routes, soil characteristics and etc [1,2]. This kind of work has only been possible via the technological advancements in hyperspectral imagery.

Various studies have dealt with identifying tree species at both pixel level and crown level. Carnegie Airborne Observatory<sup>1</sup> (CAO) is a major pioneer in employing airborne technology for remote sensing at ecology scale. Colgan et al. [2] uses a two stage Support Vector Machines (SVM) at pixel level and at crown level for tree specie classification where Light Detection and Ranging (LiDAR) measurements are used for crown segmentation. Féret and Asner [3] study the accuracy of various parametric/non-parametric supervised classification techniques and observed that there is a clear advantage in using regularized discriminant analysis, linear discriminant analysis, and support vector machines among others. There are other schools of thought which use unsupervised techniques. For example Baldeck and Asner [4] try to measure how similar beta diversity of regions are; they use distance measures such as Euclidean distance and K-means clustering. Using these clustering techniques one can provide a quick understanding of beta diversities and avoid costly and time consuming field data collections. This line of research needs more work as about 50% of pixels are classified as *other*, therefore any conclusion at this scale of uncertainty is not necessarily helpful, the same holds in Baldeck et al.'s latter work in [5].

Cho et al. [6] compares accuracies when different hyperspectral sensors of CAO, WorldView2 and QuickBird are utilized by convolving the 72 bands of CAO to eight and four multispectral channels available in the WorldView-2 and Quickbird satellite sensors, respectively. Interestingly enough they observed that WorldView-2 produced more accurate classification results than QuickBird and finally CAO. Clark et al. takes on another perspective and compares lab measurements to pixel and to crown level and try to identify important wavelength regions for specie discrimination [7]. They observed that optimal regions of the spectrum for species discrimination varied with scale. However, near-infrared (700-1327nm) bands were consistently important regions across all scales. Bands in the visible region (437-700nm) and shortwave infrared (1994-2435nm) were more important at pixel and crown scales [7]. Clark et al. in another work evaluates the effects of different metrics used for classification (indexes, derivatives, signals themselves and all together) [8]. There are other tree species classification works such as [3,9–14] that share the same approach with minor variations.

Sometimes specially tailored tools and methodologies in this field are necessary. As an example, one should note that different bands in a hyperspectral image have different signal to noise ratios, and Principal Components (PC) transform will not always result in components with a steadily increasing noise level. This makes setting a cut-off point difficult. Minimum Noise Fraction (MNF) [15] is a modified PC transform which produces a set of principal component images ordered in terms of decreasing signal quality.

---

<sup>1</sup> <http://cao.stanford.edu/>

National Ecological Observatory Network (NEON) is a long term ecology monitoring project for discovering, understanding and forecasting the impacts of climate change, land use change, and invasive species at continental-scale. National Science Foundation (NSF) provides funding for NEON as a 30-year project starting 2016. Local ecological measurements at sites distributed within 20 ecoclimatic domains across the contiguous United States, Alaska, Hawaii, and Puerto Rico will be coordinated with high resolution, regional airborne remote sensing observations [16]. Twenty terrestrial wildland core sites statistically represent unmanaged wildland conditions across the U.S.. NEON moves an additional 40 relocatable terrestrial sites every five to seven years to locations where they may best capture specific ecological phenomena such as land use change and regional nitrogen deposition. Thirty-six aquatic sites collect representative aquatic data. Many aquatic sites are located near core and relocatable terrestrial sites<sup>2</sup>. Airborne Observation Platform (AOP) would be the remote sensing platform with equipments of meter/sub-meter resolution for hyperspectral and LiDAR measurements. This paper is a pilot study on the pre-mission airborne hyperspectral data collected. No operation at the scale and time span of NEON has been ever carried out before and a thorough study of the opportunities and challenges ahead is necessary specifically in the *remote sensing* perspective where the volume of data can quickly become overwhelming [17].

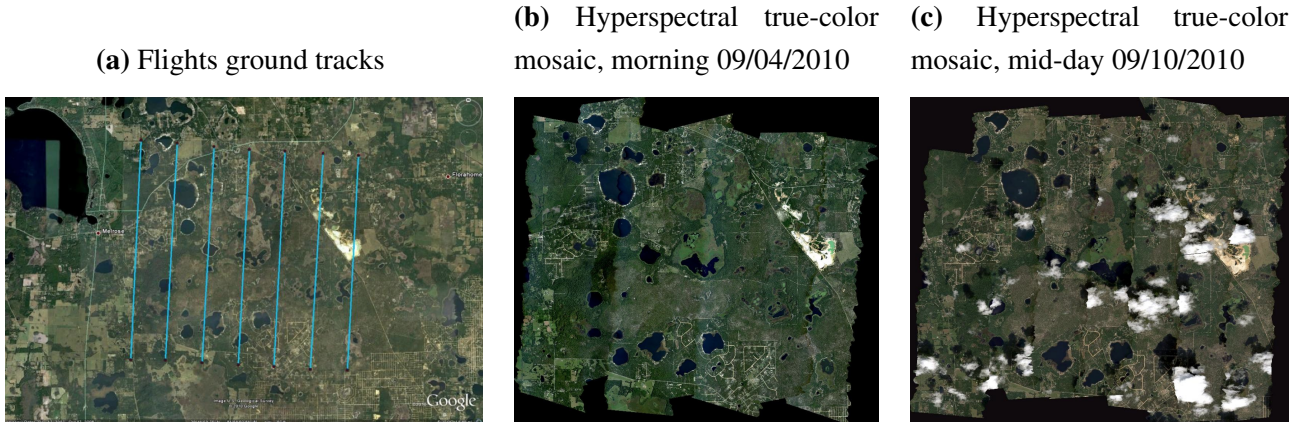
## 2. Data Collection

The NEON Southeast Domain 3 contains the southern portions of the Gulf Coast states, half of South Carolina, and all of Florida except for the southern tip. The candidate core site for Domain 3 is located at the Ordway-Swisher Biological Station (OSBS)<sup>3</sup> which is a 37-square kilometer area in Putnam County in north-central Florida and is managed jointly by the University of Florida and the Nature Conservancy located at UTM coordinates: 3,285,000 Northing, 405,000 Easting and UTM Zone 17. OSBS features diverse natural forests, small pine plantations nearby, a range of wildlife species that reflects the area's ecological communities, and a 75-year history of low human impact. Nine major plant communities exist within the region as defined by the Florida Natural Areas Inventory and these diverse targets are populated by sandhill, xeric hammock, upland mixed forest, baygalls, basin swamp, basin marsh, marsh lake, clastic upland lake and sandhill upland lakes. The sandhills community is managed using prescribed burning on a scheduled 3-year rotation. The ground sampling part of this campaign focused on a sandhill ecosystem dominated by Long-Leaf Pine (*Pinus Palustris*) and Turkey Oak (*Quercus Laevis*). The sandhill ecosystem at OSBS was selected for concurrent ground measurements because a NEON instrumented tower will be located within this ecosystem type [17,18].

Since the instrumentation slated for deployment on the eventual AOP remote sensing payloads were not yet available, airborne spectroscopic and LiDAR measurements were made during this campaign using existing systems that exhibit similar performance characteristics as the instrumentation under development [18]. It is important to note that the actual system for NEON will have better conformance of hyperspectral/LiDAR integrations and with better resolution.

<sup>2</sup> <http://www.neoninc.org/science/domains#sthash.aW1THj1N.dpuf>

<sup>3</sup> <http://ordway-swisher.ufl.edu/index.htm>

**Figure 1.** JPL AVIRIS flights over OSBS [17]

Hyperspectral: AVIRIS (Airborne Visible/Infrared Imaging Spectrometer) operated by personnel from the Jet Propulsion Laboratory (JPL) deployed on a Twin Otter DeHavilland DHC-6-300 aircraft in partnership with the National Aeronautics and Space Administration Terrestrial Ecology Program was used to collect data. JPL has flown on two separate days over OSBS: morning of September 4, 2010 (between 9:30 and 10:30 am) and mid-day of September 10, 2010. Both of the flights were flown at approximately 4000m AGL at approximately 90 knots with zenith angle of 180.0 and azimuth angle of 0.0. Details of these flights can be seen in Figure 1. Dependent on flight line, pixel size ranges from 3.3m to 3.6m. Hyperspectral data was atmospherically corrected using FLAASH [19] and ATCOR [20] algorithms. There are eight flight lines and the total size of which is 20.5GB for FLAASH and 10.2GB for ATCOR data. There are 224 bands recorded, with wavelengths from 365.93 nm to 2496.24 nm.

Atmospheric characterization relied on measurements of a CIMEL sun photometer in coordination with the NASA Aerosol Robotic Network<sup>4</sup>. Measurements were collected on September 4, 2010 and the derived atmospheric information was used to improve the atmospheric correction of the AVIRIS spectrometer data. Detailed measurements such as aerosol optical thickness, water vapor, and etc are available online<sup>5</sup>. FLAASH atmospheric correction is approximated as below [21]:

$$L_e \approx \left( \frac{(A + B)\rho_e}{1 - \rho_e S} + L_a \right) \quad (1)$$

where  $\rho_e$  is an average surface reflectance for the pixel and a surrounding region,  $S$  is the spherical albedo of the atmosphere,  $L_a$  is the radiance back scattered by the atmosphere, and  $A$  and  $B$  are coefficients that depend on atmospheric and geometric conditions but not on the surface. On the other hand, ATCOR performs atmopheric correction as follows [22]:

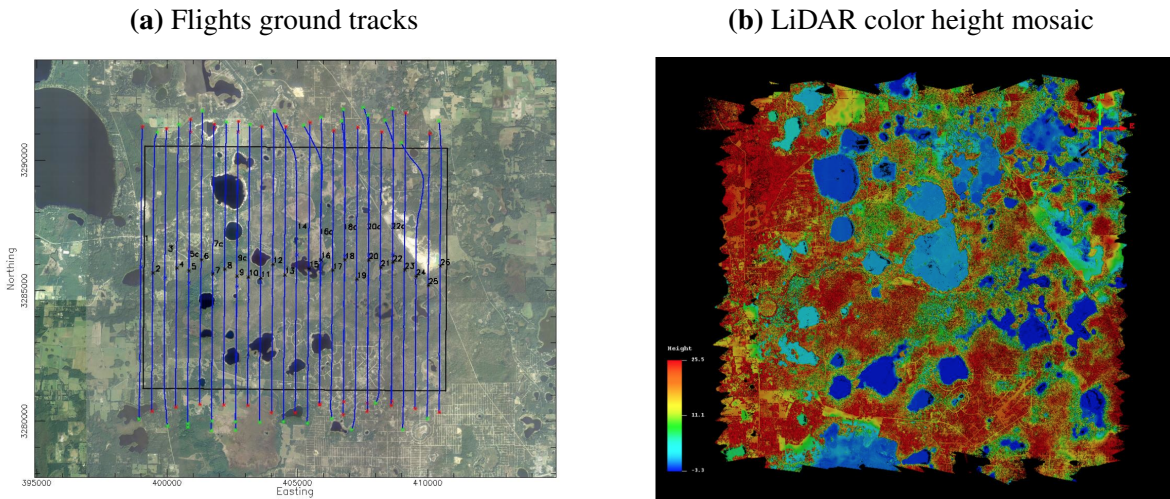
$$\rho = \frac{\pi \{ d^2(c_0 + c_1 DN) - L_{path} \}}{\tau E_g} \quad (2)$$

where  $\tau$  is the atmospheric (direct or beam) transmittance for a vertical path through the atmosphere,  $d$  is the earth-sun distance in astronomical units,  $c_0$ ,  $c_1$  and  $DN$  are the radiometric calibration offset,

<sup>4</sup> NASA AERONET: [http://gcmd.nasa.gov/records/GCMD\\_AERONET\\_NASA.html](http://gcmd.nasa.gov/records/GCMD_AERONET_NASA.html)

<sup>5</sup> OSBS Aero Measurements: [http://aeronet.gsfc.nasa.gov/cgi-bin/type\\_one\\_station\\_opera\\_v2\\_new?site=Ordway-Swisher](http://aeronet.gsfc.nasa.gov/cgi-bin/type_one_station_opera_v2_new?site=Ordway-Swisher)

**Figure 2.** NCALM Optech Gemini LiDAR flights over OSBS 09/01/2010 [17]



gain, and digital number, respectively.  $\rho$  is the surface reflectance and  $E_g$  is the global flux on the ground. You can find various measured atmospheric parameters on the OSBS Aero Measurements website.

**LiDAR:** The National Center for Airborne Laser Mapping (NCALM)<sup>6</sup> coordinated the waveform-LiDAR flights in the same study areas and as with the AVIRIS flights as displayed in Figure 2 [17]. NCALM flew an Optech Gemini<sup>7</sup> waveform-LiDAR with a nominal altitude flight covering the entire OSBS on September 1, 2010. In total there were 33 flight lines collected over OSBS both in the morning and in the afternoon, 7 flight lines were re-flown due to clouds. Range scale of LiDAR data was at 1.0m and up to five returns were recorded. The parameters for the data collected are 70 kHz PRF, wide beam divergence of 0.8 mrad, 20 deg half scan angle, and 40 Hz scan frequency. The GPS/IMU navigation data are processed using the Applanix POSPac MMS software to determine the position, orientation, and trajectory of the aircraft. The discrete LiDAR return data are processed using the Optech DASHMap software to create point cloud data files in ASPRS LAS 1.2 format [23]. Each point data record contains information such as the intensity for the laser pulse and the X, Y, and Z geolocation of the point return. DASHMap reports up to four discrete returns: first, second, third, last. Using the geolocation information, the point clouds can be visualized 3-dimensionally.

### 3. Species Classification

Upon the collection, orthorectification and atmospheric correction of hyperspectral and LiDAR data we work on identifying tree species. With the resolution of images being about 3 meters we are not getting pure pine or oak signals and there is lots of mixing going on. A pixel's hyperspectral values can be a linear/nonlinear mixing of leaf, branch, soil, shade, and other signals. The timing of flights (September) adds to the challenge: leaves might not be as green or some trees might have already started

<sup>6</sup> <http://www.ncalm.cive.uh.edu/>

<sup>7</sup> Optech Gemini LiDAR sensor: <http://www.optech.ca/gemini.htm>

**Table 1.** Field data details

Specie	ROI	Pixels per ROI	Total Pixels	Characteristics
Live Oak	4	48	85	Sand live oak ( <i>Quercus geminata</i> )
	13	37		
Turkey Oak	6	23	136	<i>Quercus laevis</i>
	7	14		
	10	73		
	11	26		
Longleaf Pine	8	7	144	<i>Pinus palustris</i>
	9	30		
	12	107		
Pine (other)	1	13	87	A mixture of different varieties of pine: Longleaf pine ( <i>Pinus palustris</i> ), Loblolly pine( <i>Pinus taeda</i> ) or Slash pine ( <i>Pinus</i> <i>elliottii</i> )
	2	30		
	3	20		
	5	24		

to lose leaves and this leads to us getting more branch signals. Further more Longleaf Pine is a conifer (needleleaf), unlike broadleaf trees where signal return can be more accurate.

### 3.1. Field Data

For our classification task, we collected ground data of identifying tree species on February 28th, 2014. We drove to OSBS with a laptop that has ArcMap installed on and the ENVI image loaded in it, we connected a professional grade GPS to the laptop. ArcMap read GPS coordinates and mapped the polygons in the ENVI image. In this way, we marked several geo-polygons that had similar plant species in the ENVI image. Later on we overlayed the identified polygons with proper JPL AVIRIS flight which had the least amount of clouds. In our situation, we bookmarked flight #4 on morning of 09/04/2010. This approach works pretty accurate if you are not in a dense forest such as tropical forests where GPS signal under the tree canopy has high deviations due to NLOS (no-line of sight) of GPS signals. Even with these considerations GPS still doesn't work that great and you need to mark several land marks such as roads, big trees and etc to be able to re-verify marked points in the map and avoid shifts in coordinates.

Altogether we identified species for 452 pixels. In Table 1 you can find the details of identified Regions of Interest (ROIs) along with their details.

### 3.2. Preprocessing

We load hyperspectral images in Matlab using an in-house upgraded version of `enviread`, initially developed by Dr. Ian Howat at Ohio State University [24]. We check for the consistency of calibration and uniformness of pixel sizes. As different flights have different altitudes and hence pixel resolutions, this is an essential step to account for. Defining a hyperspectral image  $I$  with dimensionality  $(x, y, w, z)$ , where  $x \in X$ ,  $y \in Y$ ,  $w \in W$ , and  $z \in Z$ .  $X$  represents the range of UTM Easting values,  $Y$

represents UTM Northing values,  $W = \{1, \dots, 224\}$  is the index of the reflectance wavelengths and  $Z = \{1, \dots, 60\}$  is the UTM zone of the image. Based on data, we take constant  $\xi = 10000$  as a cut-off point to avoid erroneous sensor readings. Below you can see the normalization process:

$$I_{xywz} = \begin{cases} 0 & \text{for } I_{xywz} < 0 \\ 1 & \text{for } I_{xywz} > \xi \\ \sqrt{\frac{I_{xywz}}{\xi}} & \text{otherwise} \end{cases} \quad (3)$$

There are some noises in JPL AVIRIS measurements; the range of hyperspectral reflectance values is in range  $[-32762, 32724]$ . One should note that reflectance is the proportion of sun radiance signals which should be a positive value, but in normalized form reflectance is between zero and one. To normalize we set negative reflectance values to zero and values greater than 10,000 to 10,000. To enhance the intensity of readings we take the square-root of signal returns. This procedure is due to the following facts: a) There is no standard output of reflectance data and even reflectance of a single crown at different pixels can be quite different b) We do not have ground reflectance values produced by NEON available to us c) Due to low resolution of images signals are all mixed. Due to these reasons, empirically obtained thresholds and ranges are inevitable. Regarding square root, one should note that without taking the square root the images lack proper day-light intensity and appear dark.

### 3.2.1. Filter Water Absorption Bands

In our calculations wavelengths corresponding to strong water vapor absorption bands in the atmosphere are excluded. This includes  $1333.2\text{nm}$  to  $1482.7\text{nm}$ ,  $1791.6\text{nm}$  to  $1967.4\text{nm}$ , and  $2406.9\text{nm}$  to  $2496.2\text{nm}$ . At those wavelengths, a small radiance signal is measured by the instrument due to the strong absorption, this leads to errors in the reflectance calculation (seen as a few upward spikes in reflectance plots).

### 3.2.2. Filter Non-vegetated Pixels

To properly classify tree species we get rid of pixels not belonging to planetary material, such as roads, clouds and any non-vegetated area. A good filter for this task is to use the Normalized Difference Vegetation Index (NDVI). NDVI is defined as below:

$$NDVI = \frac{NIR - VIS}{NIR + VIS} \quad (4)$$

where is  $NIR$  the reflectance in the reflective near-infrared wavelengths ( $725\text{-}1100\text{ nm}$ ) and  $VIS$  is the reflectance in the visible (red) wavelengths ( $580\text{-}680\text{ nm}$ ). The principle behind this is that  $VIS$  is in a part of the spectrum where chlorophyll causes considerable absorption of incoming radiation, and the  $NIR$  is in a spectral region where spongy mesophyll leaf structure leads to considerable reflectance [25,26]. For this purpose we chose the band at  $665.6\text{ nm}$  for red and  $734.1\text{ nm}$  for near-infrared. By filtering out pixels with  $NDVI < 0.4$  we are essentially removing pixels that are not green.

### 3.2.3. Filter Shaded Pixels

A filter of  $NIR < 0.33$  excludes heavily shaded samples which usually have distorted reflectance signals [2]. By performing previous filters we get rid of roads, clouds, shades and grassy areas and we are left with mostly tree canopies where we can apply the classification.

### 3.2.4. Gaussian Filter

Real-life sensor measurements are far from perfect and there are many noisy readings along different bands. We take advantage of abundance of bands (224 bands) and take use of their aggregated information by applying a Gaussian filter. We take a Gaussian window  $w$  of size  $N > 0$ , the coefficients of a Gaussian window are computed as below:

$$w(n) = e^{-\frac{1}{2}(\alpha \frac{n}{N/2})^2} \quad (5)$$

where  $-\frac{(N-1)}{2} \leq n \leq \frac{(N-1)}{2}$ , and  $\alpha$  is inversely proportional to the standard deviation ( $\sigma$ ) of a Gaussian random variable ( $\sigma = \frac{N}{2\alpha}$ ). Once we have Gaussian parameters we perform convolution to apply the smoothing factor. By convolving vectors  $u \in \mathbb{R}^m$  and  $v \in \mathbb{R}^n$ , we will have vector  $w \in \mathbb{R}^{m+n-1}$  such that:

$$w(k) = \sum_j u(j)v(k-j+1) \quad (6)$$

## 3.3. Support Vector Machines

It is well known in literature that Support Vector Machines (SVM) outperforms other algorithms on specie classification [2,5,6]. We perform two types of classification. We perform specie classification using *non-linear multi-class SVM* from two perspectives.

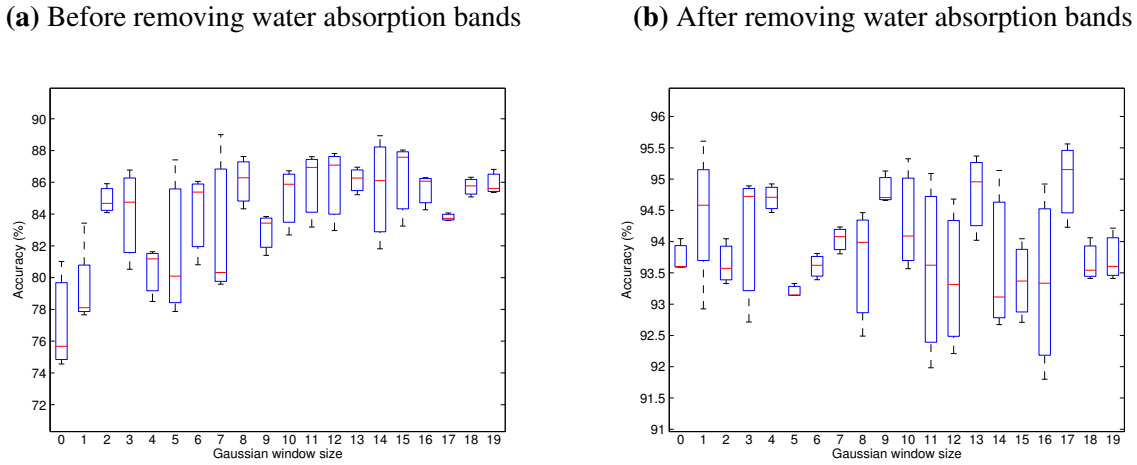
- SVM with  $\frac{2}{3}$  train,  $\frac{1}{3}$  test with no-substitution sampling.
- Perform SVM classification with  $k$ -fold cross validation where  $k = 10$ . This means we perform classification 10 times where at each time a separate non-overlapping portion of ground data is specified for train and test purposes. The ratio of train vs test is 9 to 1 from total samples.

This setup asserts the utility of cross-validation and the robustness of our approach in classification. By observing similar accuracies in cross validation runs and the  $\frac{2}{3}$  to  $\frac{1}{3}$  setup we observe that our training is robust in terms of seeing ground data and we do not have over fitting or under fitting in our trained classifier. As the field data is in order, in both of the scenarios above we shuffle the data before each run to make sure, this setup will not bias the training process.

The non-linearity comes from taking the following non-linear functions as kernel for SVM:

- Polynomial function kernel.
- Radial Basis Function (RBF) kernel

**Figure 3.** Impact of preprocessing filters on classification accuracy using polynomial kernel degree 3 on ATCOR data before and after applying pre-processing filters



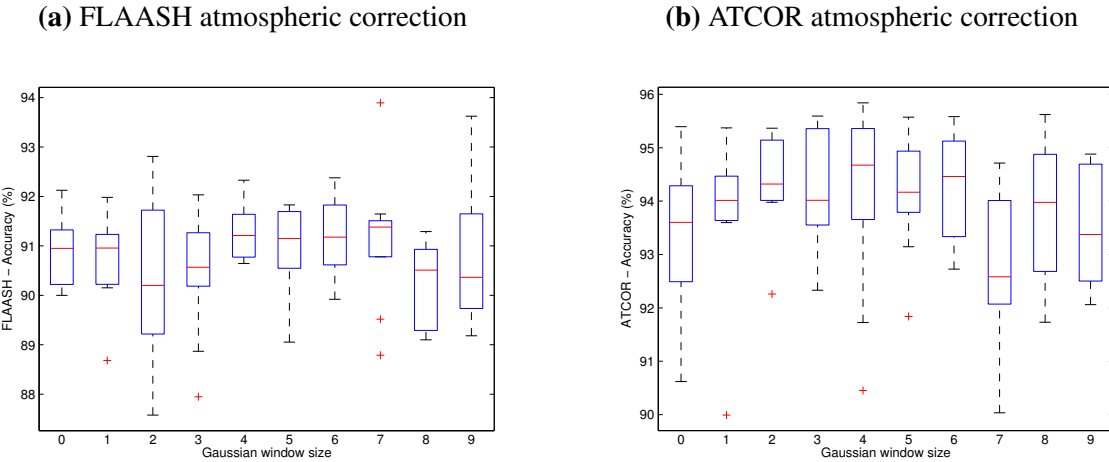
Regarding multi-class classification, we create  $\binom{c}{2}$  classifiers where  $c$  is the number of classes. We train all the classifiers and to decide on the class a given test case belongs to we do majority voting among classifiers.

#### 4. Results and Discussion

In our classification setup we first analyze the performance of our algorithm in the k-fold setup, then we show the basic  $\frac{2}{3}$  train,  $\frac{1}{3}$  test scenario and demonstrate the robustness of our classifier (which avoid over fitting/under fitting).

In k-fold scenario, first we show the effect of preprocessing filters. These analysis are done over ATCOR data with polynomial degree of 3. In Figure 3 we show how removing water absorption bands helps us improve prediction accuracy. Before removing these bands (Figure 3a) prediction accuracy starts at about 76% and rises to about 84% as we increase Gaussian window size (about 8% increase). There is a positive slope across different window sizes which means we can expect better accuracy the bigger the window size. This comes from the fact that water absorption bands add to randomness and as we increase window size this randomness is dissolved to the majority of neighbors and has less impact. After removing water absorption bands (Figure 3b), prediction accuracy starts at 93.5% and rises to about 94.5% (about 1% increase) which is minimal change but on average you can see that applying a Gaussian filter increases accuracy by small margins (maximum 1%). As window size increases you can see that there is no predictable impact of Gaussian smoothing in accuracy; sometimes it increases and sometimes it decreases accuracy as window size increases without any predictable behavior. This is due to the fact that all the currently available data has meaning and increasing window size beyond certain point just takes data away from their original meaning which can either help or harm accuracy in unpredictable ways.

Next, we look at the effect of atmospheric correction on prediction accuracy in Figure 4. As you can see in Figure 4a, FLAASH atmospherically corrected data yields 91% of prediction accuracy while Figure 4b ATCOR results in more than 93.5%. We see the same behavior of Gaussian smoothing across

**Figure 4.** Impact of atmospheric correction on classification accuracy**Table 2.** Classification Confusion Matrix using Polynomial function kernel and RBF function kernel

		Predicted Class				
Known Class	Poly \ RBF	Live Oak	Turkey Oak	Longleaf Pine	Pine (other)	
		9	0	0	0	0
Live Oak	9	0	0	0	0	0
Turkey Oak	0	10	13	0	3	0
Longleaf Pine	0	0	1	15	0	0
Pine (other)	0	0	0	0	29	7

both corrections. We see the same behavior when we analyze different parameters for the classification algorithms. As you can see in Figure 5 in the high regions of the accuracy axis, ATCOR outperforms FLAASH with a good margin. In Figure 5a at polynomial degree zero we have the maximum accuracy of prediction where ATCOR is ahead by 5%, although at degree one FLAASH improves but again we see the same performance for degrees two and three. In Figure 5b there is dominance for ATCOR data across a wide regions of  $\sigma$  in RBF function kernel.

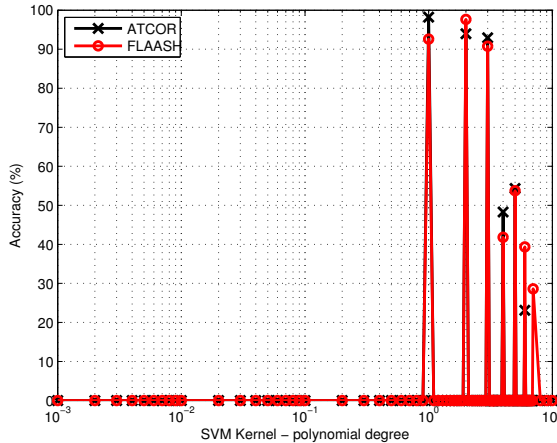
On comparing the kernel type for SVM, we see prediction accuracy of 98.26% for polynomial kernel function, and for RBF we have 93.48%. According to the confusion matrix in Table 2. In RBF, two Pine (other) pixels are confused with Longleaf Pine in RBF kernel, and one Longleaf Pine confused with Turkey Oak. On the other hand, Turkey Oak is confused to Pine (other) in Polynomial kernel

On robustness of our classification scheme from the Figure 4 and Figure 5 you can see that in the box plot, the 25th and 75th percentiles are less than 4% long in the accuracy axis. This means that our classification is always about  $\pm 2$  of the median, and that we are stable in terms of visited ground data. This is further asserted in Figure 6, where even after taking  $\frac{2}{3}$  for training and  $\frac{1}{3}$  for test, we received similar results as the k-fold scenario with 4% as the length of 25th-75th percentile.

## 5. Conclusions

**Figure 5.** Parameter tuning for classification algorithms

**(a)** Tuning polynomial order for SVM with polynomial kernel function



**(b)** Tuning  $\sigma$  in SVM with RBF kernel function

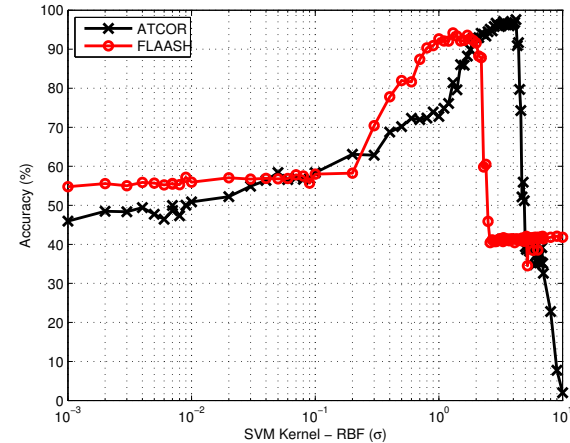
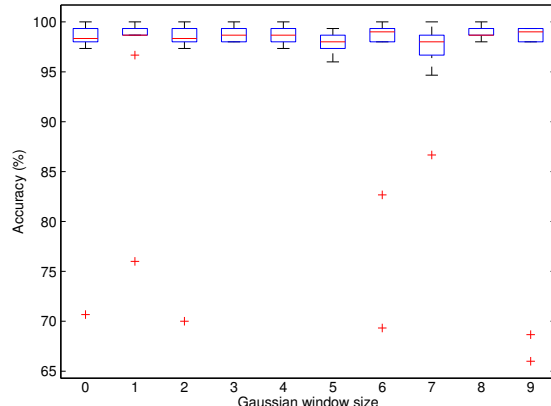


**Figure 6.** Verifying robustness of classification by applying a  $\frac{2}{3}$  training  $\frac{1}{3}$  test using polynomial kernel of degree 3



Identifying species using remote sensing technologies such as hyperspectral and LiDAR sensors has a critical utility in studying global warming, bio-mass estimation, carbon preserves, invasive species identification and etc. NEON is about to begin as a thirty-year project at continental scale with goals on ecological monitoring one of which is remote sensing. In this paper we perform specie classification using SVM over AVIRIS hyperspectral data available via NEON portal from Ordway Swisher Biological Station in north-central Florida. Our results show we can classify tree species with average 98.26% accuracy using Support Vector Machines with Polynomial function kernel of first degree. We statistically verify robustness of our classification scheme.

## References

1. Scholes, R.; Archer, S. Tree-grass interactions in savannas 1. *Annual review of Ecology and Systematics* **1997**, *28*, 517–544.

2. Colgan, M.S.; Baldeck, C.A.; Féret, J.B.; Asner, G.P. Mapping savanna tree species at ecosystem scales using support vector machine classification and BRDF correction on airborne hyperspectral and LiDAR data. *Remote Sensing* **2012**, *4*, 3462–3480.
3. Féret, J.; Asner, G.P. Tree species discrimination in tropical forests using airborne imaging spectroscopy. *Geoscience and Remote Sensing, IEEE Transactions on* **2013**, *51*, 73–84.
4. Baldeck, C.A.; Asner, G.P. Estimating Vegetation Beta Diversity from Airborne Imaging Spectroscopy and Unsupervised Clustering. *Remote Sensing* **2013**, *5*, 2057–2071.
5. Baldeck, C.; Colgan, M.; Féret, J.B.; Levick, S.; Martin, R.; Asner, G. Landscape-scale variation in plant community composition of an African savanna from airborne species mapping. *Ecological Applications* **2014**, *24*, 84–93.
6. Cho, M.A.; Mathieu, R.; Asner, G.P.; Naidoo, L.; van Aardt, J.; Ramoelo, A.; Debba, P.; Wessels, K.; Main, R.; Smit, I.P.; others. Mapping tree species composition in South African savannas using an integrated airborne spectral and LiDAR system. *Remote Sensing of Environment* **2012**, *125*, 214–226.
7. Clark, M.L.; Roberts, D.A.; Clark, D.B. Hyperspectral discrimination of tropical rain forest tree species at leaf to crown scales. *Remote sensing of environment* **2005**, *96*, 375–398.
8. Clark, M.L.; Roberts, D.A. Species-level differences in hyperspectral metrics among tropical rainforest trees as determined by a tree-based classifier. *Remote Sensing* **2012**, *4*, 1820–1855.
9. Dalponte, M.; Ørka, H.O.; Ene, L.T.; Gobakken, T.; Næsset, E. Tree crown delineation and tree species classification in boreal forests using hyperspectral and ALS data. *Remote sensing of environment* **2014**, *140*, 306–317.
10. Féret, J.B.; Asner, G.P. Semi-supervised methods to identify individual crowns of lowland tropical canopy species using imaging spectroscopy and LiDAR. *Remote Sensing* **2012**, *4*, 2457–2476.
11. Ghosh, A.; Fassnacht, F.E.; Joshi, P.; Koch, B. A framework for mapping tree species combining hyperspectral and LiDAR data: Role of selected classifiers and sensor across three spatial scales. *International Journal of Applied Earth Observation and Geoinformation* **2014**, *26*, 49–63.
12. Immitzer, M.; Atzberger, C.; Koukal, T. Tree species classification with random forest using very high spatial resolution 8-band WorldView-2 satellite data. *Remote Sensing* **2012**, *4*, 2661–2693.
13. Naidoo, L.; Cho, M.; Mathieu, R.; Asner, G. Classification of savanna tree species, in the Greater Kruger National Park region, by integrating hyperspectral and LiDAR data in a Random Forest data mining environment. *ISPRS Journal of Photogrammetry and Remote Sensing* **2012**, *69*, 167–179.
14. Ustin, S.L.; Gitelson, A.A.; Jacquemoud, S.; Schaepman, M.; Asner, G.P.; Gamon, J.A.; Zarco-Tejada, P. Retrieval of foliar information about plant pigment systems from high resolution spectroscopy. *Remote Sensing of Environment* **2009**, *113*, S67–S77.
15. Green, A.A.; Berman, M.; Switzer, P.; Craig, M.D. A transformation for ordering multispectral data in terms of image quality with implications for noise removal. *Geoscience and Remote Sensing, IEEE Transactions on* **1988**, *26*, 65–74.

16. Kampe, T.U.; Johnson, B.R.; Kuester, M.; Keller, M. NEON: the first continental-scale ecological observatory with airborne remote sensing of vegetation canopy biochemistry and structure. *Journal of Applied Remote Sensing* **2010**, *4*, 043510–043510.
17. Krause, K.; Kuester, M. Airborne Observation Platform (AOP) Pathfinder 2010 Data Release. <http://neoninc.org/pds/files/NEON.AOP.015068.pdf>. The National Ecological Observatory Network is a project sponsored by the National Science Foundation and managed under cooperative agreement by NEON, Inc. The NEON 2010 Pathfinder data set is based on work supported by the National Science Foundation under Grant DBI-0752017.
18. Kampea, T.; Krausea, K.; Meiera, C.; Barnetta, D.; McCorkela, J. The NEON 2010 Airborne Pathfinder Campaign in Florida, 2010. NEON Technical Memo 002.
19. Adler-Golden, S.; Berk, A.; Bernstein, L.; Richtsmeier, S.; Acharya, P.; Matthew, M.; Anderson, G.; Allred, C.; Jeong, L.; Chetwynd, J. FLAASH, a MODTRAN4 atmospheric correction package for hyperspectral data retrievals and simulations. Proc. 7th Ann. JPL Airborne Earth Science Workshop, 1998, pp. 97–21.
20. Richter, R.; Schläpfer, D. Atmospheric/topographic correction for satellite imagery. *DLR report DLR-IB* **2005**, pp. 565–01.
21. Adler-Golden, S.M.; Matthew, M.W.; Bernstein, L.S.; Levine, R.Y.; Berk, A.; Richtsmeier, S.C.; Acharya, P.K.; Anderson, G.P.; Felde, J.W.; Gardner, J.; others. Atmospheric correction for shortwave spectral imagery based on MODTRAN4. SPIE's International Symposium on Optical Science, Engineering, and Instrumentation. International Society for Optics and Photonics, 1999, pp. 61–69.
22. Richter, J.; Schläpfer, D. Atmospheric / Topographic Correction for Satellite Imagery. ATCOR-2/3 User Guide, Version 8.3.1, February 2014. ATCOR, 2014.
23. LAS Specification Version 1.2. [http://www.asprs.org/a/society/committees/standards/asprs\\_las\\_format\\_v12.pdf](http://www.asprs.org/a/society/committees/standards/asprs_las_format_v12.pdf). Approved by ASPRS Board 09/02/2008.
24. Howat, I. ENVI file reader, updated 2/9/2010. <http://www.mathworks.com/matlabcentral/fileexchange/15629-envi-file-reader--updated-2-9-2010>. This code initially developed by Ian Howat, and updated by Yushin Ahn, Ray Jung and CSI lab University of Florida.
25. Tucker, C.J. Red and photographic infrared linear combinations for monitoring vegetation. *Remote sensing of Environment* **1979**, *8*, 127–150.
26. Jackson, R.; Slater, P.; Pinter Jr, P. Discrimination of growth and water stress in wheat by various vegetation indices through clear and turbid atmospheres. *Remote sensing of environment* **1983**, *13*, 187–208.